The dynamic response of offshore wind turbines and their sensitivity to wind field models

The dynamic response of offshore wind turbines and their sensitivity to wind field models

Maylinn Haaskjold Myrtvedt, Astrid Nybø and Finn Gunnar Nielsen

Geophysical Institute, and Bergen Offshore Wind Centre (BOW), University of Bergen, Norway

E-mail: mayhmyr@gmail.com

Abstract. As the rotor diameter of offshore wind turbines increases, an improved understanding of the structure of the turbulent wind field approaching the rotor is important. Present standards for computing wind loads are resting upon assumptions of neutral atmospheric conditions and a simplistic formulation of the coherence of the turbulence. In the present work, various formulations of the wind field are applied and the dynamic responses of a bottom fixed and a floating wind turbine are computed to investigate the sensitivity to the formulation of the wind field. Focus is on wind situations with above average turbulence intensity as these are expected to have a significant contribution to fatigue damage of the structure. It is observed that choice of wind spectrum, coherence formulation as well as assumptions related to atmospheric stability conditions significantly influences the dynamic loads in tower bending moment, yaw moment and blade flap moment. The differences are significant in particular in the low frequency range. This implies that in particular floaters are sensitive to the formulation of the wind field.

1. Introduction

Knowledge of offshore wind characteristics are essential when investigating offshore wind turbine structures. The present study is based on an extensive analysis of wind data obtained from the offshore research platform FINO1 located in the North Sea [1]. The data analysis is described and discussed in Nybø et al. [2]. This study considered field data from sonic anemometers obtained over a period of more than one year.

Eliassen and Obhrai [3] also used data from FINO1, specifically to study coherence of turbulent wind. This study considered measurements obtained over one month and for neutral conditions only. Yet it found large differences between coherence of measured values and the coherence functions recommended in standards for wind turbine design. In the study of Nybø et al. [4] and the present study, the coherence of turbulent winds is further investigated for a few cases with unstable, neutral and stable atmospheric conditions. Within each of the stability classes considered (unstable, neutral and stable), large variations of turbulence intensities (TI) are observed in the data [4]. Nybø et al. [4] focused on average TI situations, while we focus on situations where the TI is higher than average. Situations with high TI level are expected to contribute significantly to structural fatigue. It is thus important to investigate if dynamic response is sensitive to the atmospheric stability in situations with high TI level.

The impact of the various wind characteristics on both a bottom fixed and a floating wind turbine is considered in the present study. The 10 MW DTU reference turbine [5] is placed on a monopile and a

spar foundation. When analysing the dynamic response of bottom fixed turbines, the industry standard is to use stationary wind conditions of ten minutes duration. As floating wind turbines have natural periods up to the range of minutes, much longer periods must be considered to obtain reliable statistics of the response. In the study by Nybø et al. [4], cases with fairly stationary wind conditions over one hour are identified. The choice of one hour duration for the analysis is a compromise between what can be expected to be the duration of fairly stationary conditions in the field data and the need for reliability of the statistical estimates. In the present study, we consider three situations of one hour duration. The average wind speeds chosen are below rated, close to rated and above rated wind speed. Together with the three stability classes, nine cases are thus studied.

Godvik [6] used the two turbulent wind field methods recommended by the IEC wind turbine design standards [7–9] for load simulations of offshore wind turbines. The methods recommended in the standards are challenged by the increased rotor sizes and the introduction of floating substructures having much lower natural frequencies than bottom fixed. Godvik M. [6] conclude that it is important to improve and validate the standard wind models to reduce uncertainty, in addition to the need of comparing site specific models with standardized models. The current study has used the actual measured time histories of the wind speed as input to generate turbulent wind fields, in addition to the two wind field methods recommended by the IEC wind turbine design standard, for load simulations of offshore wind turbines. This approach allows for evaluation of the standard models, in addition to the possibility of gaining a better understanding of site specific impact on the turbine response. To sum up, wind fields of the nine mentioned cases are simulated using three wind field generation methods.

The aerodynamic loads on the turbine are computed and the bending moments at the blade root, the bottom and the top of the tower are investigated. The tower top yaw moments are also studied.

The present study is considered as an introductory work to illustrate the importance of atmospheric stability, turbulence and coherence model to the loads on large diameter offshore wind turbines. It aims to demonstrate that these parameters are of significant importance through the comparison of the impact from the three mentioned wind field methods on the response. This work focuses on highlighting the differences between the wind fields, while further work will address which model gives the most realistic results.

2. Wind turbine simulation

2.1. Wind fields

Throughout this paper, the wind field situations will be referred as “7.5 m/s”, “12.5 m/s” and “17.5 m/s” for the below rated, close to rated and above rated cases respectively.

For each of the nine cases, three turbulent wind fields are generated. The two wind field models recommended by the IEC wind turbine design standards [7–9] are used; the Mann uniform shear model and the Kaimal spectral model. In the following denoted “Mann” and “Kaimal” respectively for short. In the Kaimal model, an exponential coherence function is applied while generating the wind field. The third method, TIMESR, uses measured wind velocity time series as input. The time series used are obtained from the FINO1 platform measured at three different vertical locations. An exponential coherence function (Davenport [10]) with coefficients computed from measurements is used in this study, see Nybø et al. [2, 4] for details.

For each of the nine cases, the three generated wind fields have similar turbulence intensity and vertical shear profile. Thus, the turbulence intensity and shear profile are removed as causes for differences in the computed dynamic responses of the wind turbines. For detailed explanation of the procedure followed, see [4, 11].

Time series with wind speeds at about 7.5 m/s, 12.5 m/s and 17.5 m/s are found from the quality assured offshore wind dataset discussed in [2]. Figure 1 illustrates the range of TI levels as well as stability conditions for cases with wind speeds about 12.5 m/s. Stability is classified using the Obukhov length with ranges from Van Wijk et al. [12], see Table 1. When choosing situations, only one stable

and one unstable situation is chosen for each wind speed, in order to keep the number of wind fields and load cases at a manageable level. The Obukhov lengths are calculated based on meteorological data from the sonic anemometer at 40 m, for details see Nybø et al. [4].

As mentioned in the introduction, cases with high TI level is expected to significantly contribute to structural fatigue. In the present study, cases with TI level above the 90 percentiles are thus chosen for further use. From Figure 1 it is observed, as expected, that the TI level for unstable conditions in general is higher than for neutral and stable conditions. In Table 2 the parameters obtained from the chosen cases used in the generation of the twenty-seven (nine situations and three generation methods) wind fields are given. At 12.5 m/s, the chosen unstable situation is very turbulent, which is desirable in this study. There are far less available situations to choose from at higher wind speeds. Generally, the TI decreases with an increased mean wind speed, as observed from Table 2, the 17.5 m/s cases have somewhat lower TI than the 12.5 m/s cases.

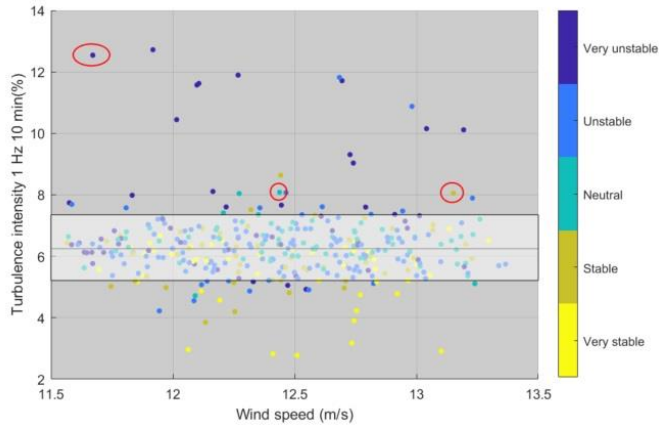

Figure 1. TI level for cases with wind speeds around 12.5 m/s. The color coding indicates the atmospheric stability condition**.** The three cases encircled are used in the dynamic analysis.

Table 1. Stability classification after Van Wijk et al. [12]

Stability	**Range**
Very stable	0<L<200 m
Stable	200<L<1000 m
Neutral	|L|>1000 m
Unstable	-1000<L<-200 m
Very unstable	-200<L<0 m

In the Mann field, turbulence intensity is included in the calculation of the dissipation rate of turbulent eddies, $\alpha\epsilon^{2/3}$. α is the three-dimensional Kolmogorov constant and ϵ is a measure of the energy dissipation. The dissipation rate is expressed as [7]:

$$\alpha\epsilon^{2/3} = \frac{55}{18} \cdot 0.4754 \cdot \sigma_{iso}^2 \cdot L_M^{-\frac{2}{3}}, \quad (1)$$

where the IEC wind turbine design standard describes the isotropic variance as $\sigma_{iso} = 0.55 \cdot \sigma_u$. The standard deviation, σ_u, includes characteristics from the measurements as it is obtained from the wind measured at 80 m. For the shear distortion parameter, $\Gamma = 3.9$ (also used in the Mann model), and turbulence length scale, $L_M = 33.6$ are used. These are the values recommended by the IEC [7–9]. Others, e.g. Sathe et al. [13], have observed variation of these parameters depending upon the atmospheric conditions. Γ and L_M may impact on the fatigue load. This has not been considered in the present work as our motivation was to compare standard models with standard inputs as used by the industry with wind fields based upon realistic offshore time series for wind turbine simulation.

Table 2. Measured wind parameters used for generation of the turbulent wind fields

Below rated (approx. 7.5 m/s)			***Close to rated (approx. 12.5 m/s)***			***Above rated (approx. 17.5 m/s)***		
Neutral	**Stable**	**Unstable**	**Neutral**	**Stable**	**Unstable**	**Neutral**	**Stable**	**Unstable**
Turbulence intensity (%)								
7.53	8.21	9.13	8.08	8.05	12.54	7.58	7.58	8.77
Mean wind speed (m/s)								
7.92	7.47	7.53	12.44	13.15	11.67	16.79	17.61	18.00
$\alpha\epsilon^{2/3}$								
0.013	0.015	0.021	0.040	0.043	0.094	0.071	0.077	0.098

Each wind field generated has a square cross-sectional extent which covers the rotor plane with some margin, i.e. a square section with width 224 m centered at the hub level. The wind fields are computed at 64 by 64 grid points at each cross-section. The duration of the wind fields are 3800 seconds, allowing for a 200 seconds transient start-up period in each dynamic simulation.

The Kaimal and TIMESR wind fields are generated using the turbulence simulator, TurbSim [14]. Except for the TI taken from the chosen time series, illustrated in Figure 1, standard parameters are also used in the generation of the Kaimal wind fields. The DTU Mann generator [15] is used to create three-dimensional wind boxes, by implementing 32768 grid points in the longitudinal direction, based on the Mann turbulence model. Taylor's hypothesis of "frozen turbulence" [16] is assumed when "pushing" this wind box through the wind turbine. The wind box of the Mann generator and the yz planes at a number of time slices of TurbSim are illustrated in Figure 2.

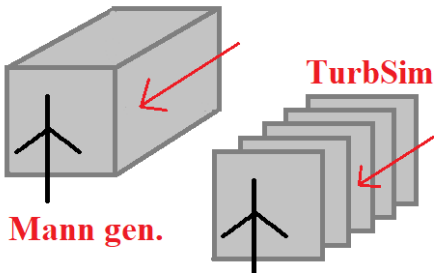

Figure 2. Wind box (Mann generator) and yz planes (TurbSim).

In the standard methods, the power law, with the shear exponent calculated from the various measurement situations, is used to determine the vertical mean wind speed. The logarithmic law is used together with the TIMESR method. See detailed description of the procedure in [4] or [11].

2.2. Tool for dynamic analysis

The SIMA program suite (described in [17]), is used for the dynamic calculations. A Beam Element Momentum (BEM) method is used for computing the aerodynamic loads. To demonstrate the effect of the various wind field formulations as clear as possible, waves and wave loads are omitted in the present study.

2.3. Wind turbine models

In the present study, the DTU 10 MW horizontal axis reference wind turbine (hereafter denoted RWT) [5] is used both for the bottom fixed and floating substructure. The turbine blades, tower and monopile are all modelled as flexible structures, while the floating substructure is modelled as a rigid, floating body. Some of the key parameters of the RWT are summarized in Table 3.

Table 3. The main properties of the DTU 10 MW reference turbine (RWT)

Parameter	**DTU 10 MW RWT**
Rated power	10 MW
Rated wind speed	11.4 m/s
Number of blades	3
Rotor diameter	178.3 m
Hub height above sea level	119 m
Minimum rotor speed	6.0 rpm
Maximum rotor speed	9.6 rpm
Control	Variable speed, Collective pitch

This land-based reference turbine, with some modifications related to inner blade foils and a stiffened tower as explained in Sørum et al. [18, 19], is placed upon a monopile with dimensions as described by the same references. In the present implementation, the rotor mass is 1.2 % larger than the RWT and the tower mass is 3.9 % larger.

The same turbine and tower are placed upon a spar substructure. The spar substructure is based upon the dimensions proposed by Xue [20], with some adjustments related to damping estimates and mass reduction of the substructure to float at correct draft [11]. The main particulars are given in Figure 3. The total mass of the floating turbine is 13016 t where 11731 t correspond to the spar substructure including ballast.

The natural frequencies for the bottom fixed turbine are reported by Sørum et al. [18] and reproduced in Table 4. To find the natural frequencies for the rigid body motions of the floater, numerical decay tests with no wind and calm water were performed in SIMA. The results are shown in Table 5.

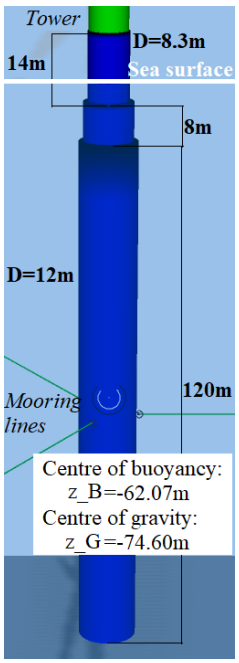

Figure 3. The spar substructure with main dimensions.

Table 4. Natural frequencies obtained for the bottom fixed turbine, as obtained by Sørum et al. [18].

Mode	Natural frequency [Hz]
1st Tower side-side mode	0.227
1st tower fore-aft mode	0.228
1st blade asymmetric flapwise (yaw)	0.564
1st blade asymmetric flapwise (pitch)	0.594
1st collective flap mode	0.624
1st asymmetric edgewise1	0.951
1st asymmetric edgewise2	0.957
2nd tower side-to-side	1.303
2nd tower fore-aft	1.189
2nd asymmetric flapwise (yaw)	1.460
2nd asymmetric flapwise (pitch)	1.682

Table 5. The natural periods for rigid body motions of the floater and associated damping level

Mode	Natural periods (s)	Description	Damping ratio (%)
Surge	134.4	Translation in x-direction	6
Sway	135	Translation in y-direction	6
Heave	31.5	Translation in z-direction	2
Roll	40	Rotation about the x-axis	4
Pitch	40	Rotation about the y-axis	5
Yaw	10.2	Rotation about the z-axis	100

The hydrodynamic damping for the rigid body motions are specified as a combined linear and quadratic damping. The linear damping contributes to numerical stability at small amplitudes of oscillations, while the quadratic damping provides a proper estimate of the viscous damping at realistic motion amplitudes. The damping ratios given in Table 5 correspond to the linearized damping obtained at amplitudes of oscillation 3 m for surge and sway; 6 Deg. for pitch and roll and 2 m for heave. As the present combination of aerodynamic loading and control model in some cases may cause build-up of large yaw motions, and as the yaw motions were not part of the present study, an artificial large yaw damping was used. If a floater does not have a sufficient yaw damping, damping may be introduced via individual blade pitch control.

In this study, an updated version of the controller developed by DTU Wind Energy [21] is used for both turbines. Some adaptions were performed for the floating system to avoid controller induced instabilities. This implies shifting the natural frequency of the blade pitch controller to lower frequencies, see [11] for further details.

3. Results and discussion

3.1. The generated wind turbulence

To compare frequency distribution of the turbulence for the various wind field generation methods, the turbulence spectra at the nacelle level are computed. Examples of the computed spectra are shown in

Figure 4 for wind speeds close to 12.5 m/s. The spectra as obtained by Mann, Kaimal and TIMESR, show expected similarities of turbulence level as the three methods have the same TI within each atmospheric stability condition. All spectra follow the theoretical turbulence decay (Kolmogorov) for the mid-to-high frequency range. In the low-frequency range, less than 0.1 Hz, differences appear between the different stability classes. These differences are related to the differences in TI, where unstable conditions correspond to higher energy levels than stable. In this low frequency range, which is especially relevant for floaters, some differences between the three spectral methods are also observed. It should be mentioned that the statistical uncertainty is larger in this region due to fewer samples.

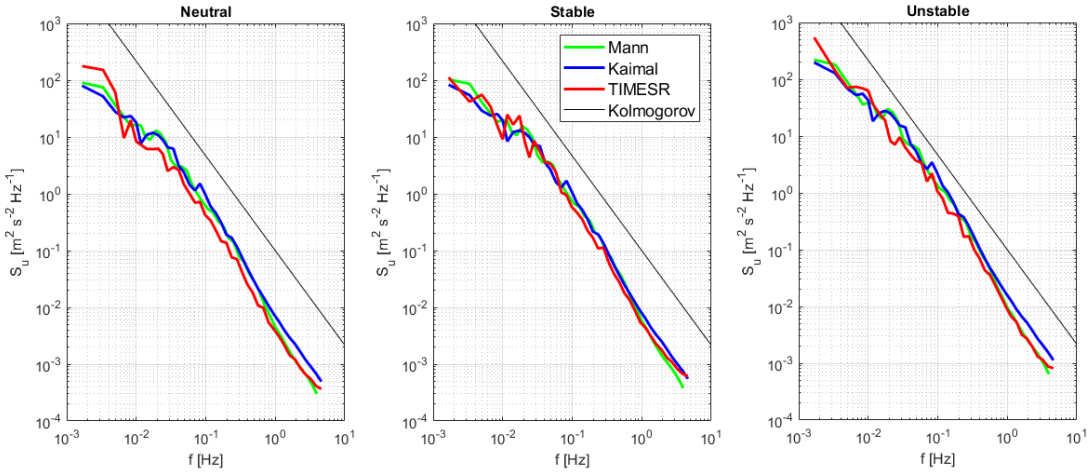

Figure 4. The power spectral density at hub centre for the along wind component (u) at 12.5 m/s mean wind speed. Atmospheric stability: neutral (left), stable (centre) and unstable (right). The three different spectral generation methods; Mann, Kaimal and TIMESR are represented by different colours.

The spatial variation of turbulence in the wind field is expressed by the coherence. The present work considers variations in the along wind speed (u) only. Coherence is a function of the mean wind speed, U, the frequency, f, and the separation distance between the points considered, r. These parameters are combined into a non-dimensional frequency, the reduced frequency, given by $\frac{fr}{U}$. The coherence, γ_{xy}, for a separation distance between two points, x and y, are defined by the auto (S_x and S_y) and cross (S_{xy}) spectral densities of the turbulent fluctuations:

$$\gamma_{xy}(f) = \frac{S_{xy}(f)}{\sqrt{S_x(f) \cdot S_y(f)}} = Co_{xy}(f) + iQu_{xy}(f). \tag{2}$$

Here, Co_{xy} and Qu_{xy} are the real and imaginary part of the coherence, denoted co-coherence and quad-coherence respectively. The Davenport (used in TIMESR) and IEC coherence model (used in Kaimal) assume the coherence to be real and positive. This is in contrast to the Mann model and measurements where a complex coherence is obtained for vertical separation distances. In the Mann model the quad-coherence is caused by the vertical shear. The quad-coherence as function of reduced frequency, as obtained by the Mann model and from the measurements are illustrated in Figure 5. It is worth noticing that even though the co-coherence is dominant, the quad-coherence is significant, causing a phase shift which is expected to influence dynamic response in wind turbine simulation.

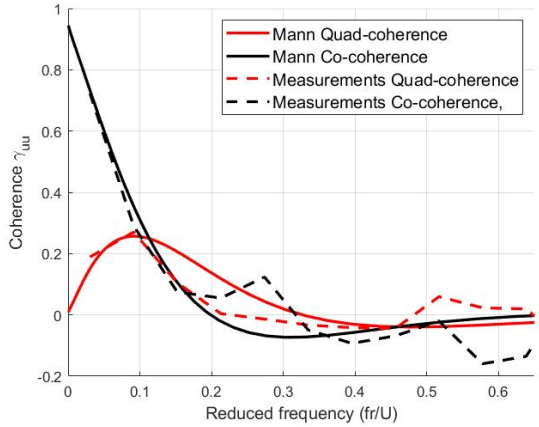

Figure 5. Quad- and co-coherence for the u-component and 40 m vertical separation distance. Mann and measurements for 12.5 m/s mean wind speed in stable atmospheric condition.

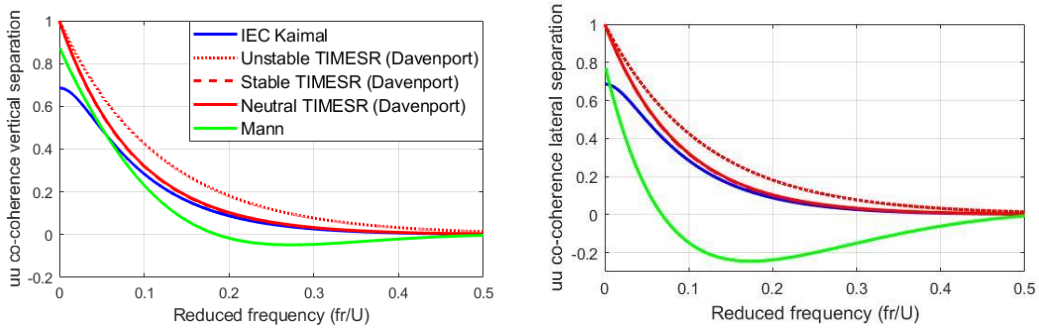

Figure 6. Co-coherence of the u-component for 12.5 m/s mean wind speed. ½D vertical (left) and lateral (right) separation distance. Results obtained by the Kaimal, TIMESR and Mann formulations. Note that the stable and neutral TIMESR have similar curves due to small differences in decay coefficients.

Figure 6 illustrates the co-coherence in 12.5 m/s wind flow between points separated vertically and laterally at half a rotor diameter (89.15 m). As expected, and also pointed out by Panofsky and Singer [22], high-frequency fluctuations have low coherence. The co-coherence generated by the standard method, Kaimal, is close to the results as obtained from TIMESR in neutral conditions. This is valid both for vertical and lateral separation. The similarity is to be expected given the similarity in the decay coefficients used in the coherence models. One should note the negative values obtained in the co-coherence both by the Mann model and from the observations in Figure 5. These negative values imply an opposite phase of the turbulent fluctuations, potentially having significant impact on the aerodynamic loads. For further discussion on the observed versus modelled coherence, reference is made to Nybø et al. [4].

3.2. Load response

Load analysis for the bottom fixed and the floating turbine is performed using the wind fields discussed above. Below, a few key responses are presented. The focus has been on the global responses on tower top and bottom bending moments (TTBM and TBBM) and the local response flapwise bending moment on a blade (FBM). Additionally, the tower top yaw moment (TTYM) is investigated as the various wind field formulations generate wind fields with different spatial distribution which may cause differences in the yaw loads. To have a robust load parameter relevant for fatigue, the standard deviations of the

loads are considered. Load spectra for the 12.5 m/s wind speed cases are presented as well. More details are found in Myrtvedt [11].

3.2.1. Tower bottom fore-aft bending moment. A significant variation in the standard deviation of the TBBM is observed, both by comparing the different stability classes and the methods for generating the wind fields. This is illustrated in Figure 7. In agreement with Bachynski and Eliassen [23], one can see clear differences in the response depending on which pre-generated wind field is used as input for the turbine simulation.

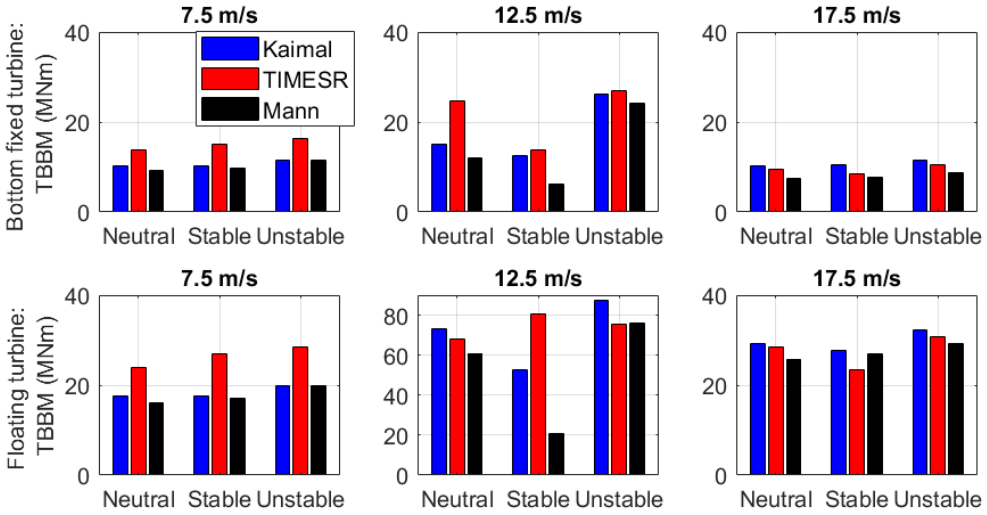

Figure 7. Standard deviation of tower bottom fore-aft bending moment (TBBM) in MNm. Results by considering various atmospheric stabilities and wind field simulation methods. 7.5 m/s (left), 12.5 m/s (centre) and 17.5 m/s (right) mean wind speeds. Bottom fixed turbine (top) and floating turbine (bottom).

TBBM is dominated by the variation in turbine thrust times the tower height and is less sensitive to the local variation in wind velocity over the rotor area. This means that the TBBMs are not strongly influenced by the coherence which are consistent with what Dimitrov et al. [24] observed.

The largest standard deviations are observed for the 12.5 m/s cases as expected, given the high thrust levels at rated wind speed. Here also the largest differences between the different wind spectral methods are observed. For the bottom fixed turbine, the TIMESR gives the largest response in all stability classes. Unstable atmospheric conditions give in general larger response than the neutral and stable. This is to be expected from the TI levels. An interesting observation is the large differences between the methods in neutral conditions for the bottom fixed turbine. As the spectral models has neutral condition as an inherent assumption, one may expect less variation in this condition. The floating wind turbine have significant larger TBBMs than the bottom fixed. This may be explained by the platform pitch motions and corresponding acceleration and gravity loads. The contribution comes from frequencies close to the natural frequency in pitch (0.025 Hz).

The 7.5 m/s case in Figure 7 show similar trends across the methods for both turbines, where TIMESR points out to give highest bending loads and the standard methods gives about the same standard deviation. For the 17.5 m/s wind speed, none of the methods systematically gives highest bending moment. The unstable conditions also at this wind speed shows somewhat higher response than the neutral and stable cases. This should be expected from the somewhat higher turbulence level.

In Figure 8 examples of the load spectra for the TBBM are presented for the bottom fixed and floating turbines. A general observation is that the largest spectral values as well as the largest differences between the wind generation methods are found in the low frequency range (below 0.5 Hz). This is consistent with the analysis of the wind field spectra presented in Figure 4. In particular in the stable conditions, the Mann method corresponds to lower energy levels. This is consistent with the low standard deviations shown in Figure 7. The peaks in the spectra at 0.23 Hz corresponds to the 1st tower fore-aft bending mode, while the peak just below 0.5 Hz correspond to 3 times the rotor frequency (3P). The peak at just below 1 Hz is close to the edgewise natural frequency. It is not obvious why this mode should influence the TBBM. The 2nd tower fore-at bending mode has a somewhat higher natural frequency. The floating wind turbine has considerable larger response than the bottom fixed at very low frequencies, in particular at 0.025 Hz, caused by the platform pitch motion. Also, a larger response at the 3P frequency is observed for the floater.

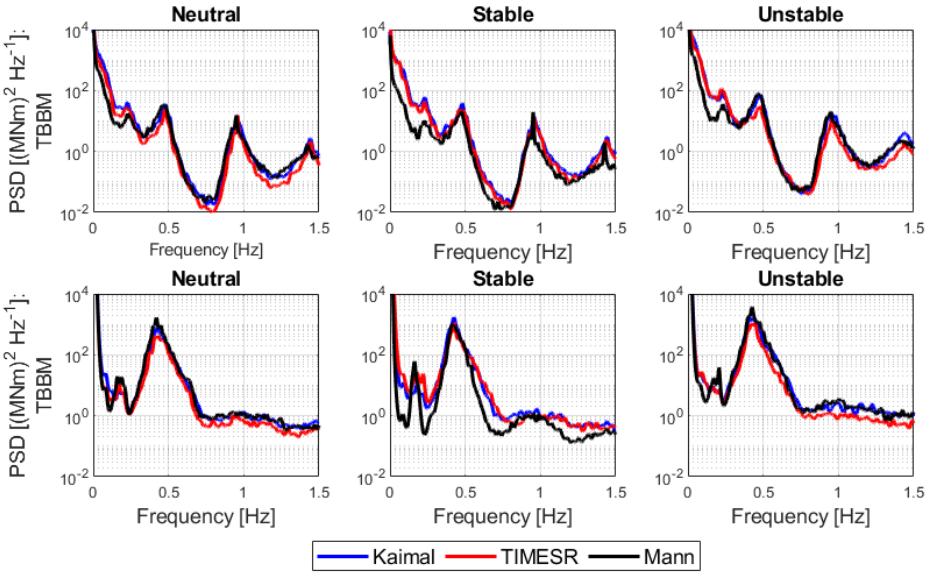

Figure 8. Load spectra for tower fore-aft bending moment at the tower bottom (TBBM) for 12.5 m/s mean wind speed. Bottom fixed turbine (top) and floating turbine (bottom). Neutral (left), stable (centre) and unstable (right) atmospheric conditions.

3.2.2. Tower top fore-aft bending moment. It is expected that the tower top bending moment is more sensitive to coherence than TBBM analysed above. The TTBM is also influenced by wind shear, but the shear is similar across the wind generation methods. The coherence of Mann is less significant than for the other methods (Figure 6). In agreement with Doubrawa et al. [25], we thus expect correspondingly increasing loads due to the spatial heterogeneity of Mann. However, this is not found in the TTBM results shown in Figure 9. The platform pitch motion does not contribute to the TTBM, resulting in less difference between the results for the bottom fixed and the floating wind turbine. From Figure 9 it is also observed that the variations between the results using the various wind field generation methods, are less than for the TBBM.

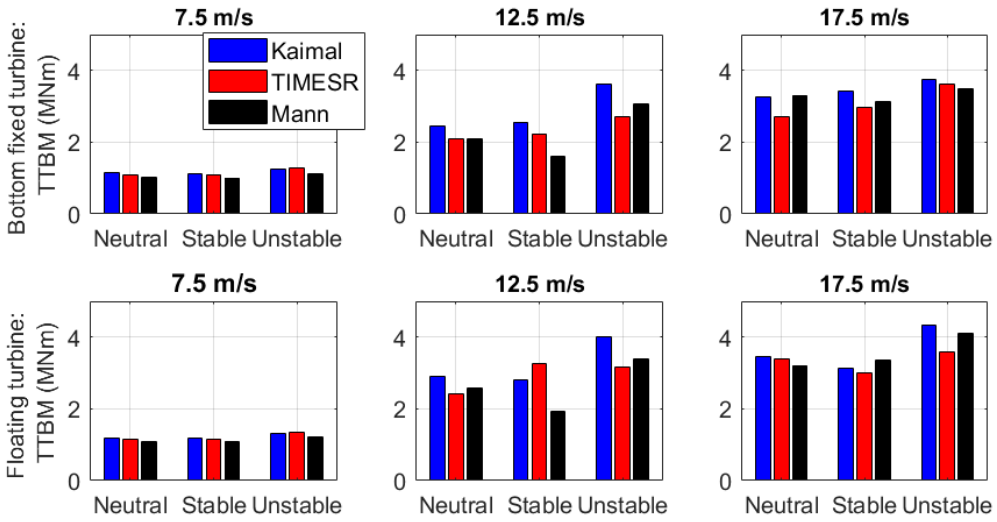

Figure 9. Standard deviation of tower top fore-aft bending moment (TTBM) in MNm. Results by considering various atmospheric stabilities and wind field simulation methods at 7.5 m/s (left), 12.5 m/s (centre) and 17.5 m/s (right) mean wind speeds. Bottom fixed turbine (top) and floating turbine (bottom).

In Figure 10 examples of the load spectra for the TTBM are presented for the bottom fixed and the floating turbine respectively. For the bottom fixed turbine, the results are in general fairly similar for the three wind generation methods used. The most peculiar feature of these spectra are the distinct peaks. The narrow peak at 0.16 Hz corresponds to 1P (constant rotational speed of the rotor); 0.48 Hz to 3P; 0.95 Hz and 1.46 Hz corresponds to various blade modes, see Table 4. The spectra for the TTBM of the floater are very different due to the different eigenfrequencies (Table 4 and 5). The damping formulation may also impact the results. The damping of the tower and blade modes is very low in the case of the bottom fixed turbine. For the floating turbine, significant hydrodynamic and controller damping is present. This may remove most of the resonant responses observed for the bottom fixed turbine. Even if the resonant responses are clearly visible at the logarithmic scale, the contribution to the standard deviation is not very significant. The load spectra for the floating turbine in Figure 10 show that both 1P frequency (0.16 Hz) and the 3P frequency (0.48 Hz) are observed in all stability cases. The 3P frequency has blade modes in close vicinity.

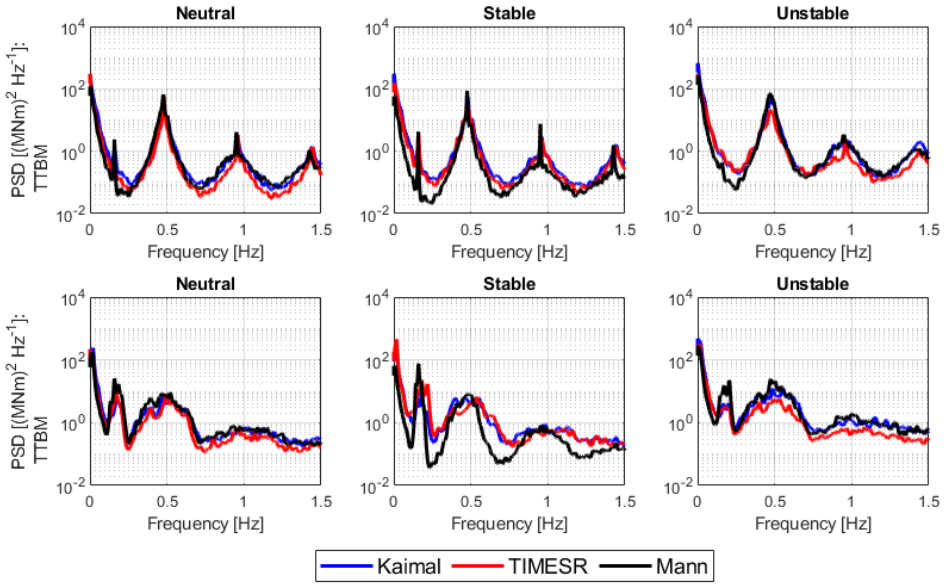

Figure 10. Load spectra for fore-aft bending moment in the tower top (TTBM) for 12.5 m/s mean wind speed. Bottom fixed turbine (top) and floating turbine (bottom). Neutral (left), stable (centre) and unstable (right) atmospheric conditions.

3.2.3. Flap-wise bending moment. The standard deviation of the computed blade root flap-wise bending moments (FBM) are shown in Figure 11. There are not very large differences between the bottom fixed and the floating turbine for the 7.5 m/s and 17.5 m/s wind speed cases. Again, the largest values and variations between the methods employed are observed for the 12.5 m/s wind speed cases where the loads are highest. The standard deviation of the flap-wise bending moment at the 12.5 m/s wind speed is larger for the floating turbine than the bottom fixed. Both the platform motions and the differences in the controller settings may contribute to this result. Sathe et al. [13] hypothesize that the dynamic moments at the root section are mainly influenced by the wind profile and turbulence. Wind shear causes stress in the cross sections of the blades and the stresses increases moving towards the sections near the rotor. Sathe et al. [13] observed that the bending loads in the root section influenced by atmospheric stability was not notably. In our case this is also the case for the 7.5 m/s wind speed simulations. We see larger differences between the different stabilities at higher wind speeds, but this may also originate from varying wind profiles and TI's at the various stabilities. At 12.5 m/s we see differences due to the choice of wind field generation method. We observe that the TIMESR formulation give the highest standard deviation in most cases, especially at 7.5 m/s. At 17.5 m/s wind speed, the stable case gives the highest loads.

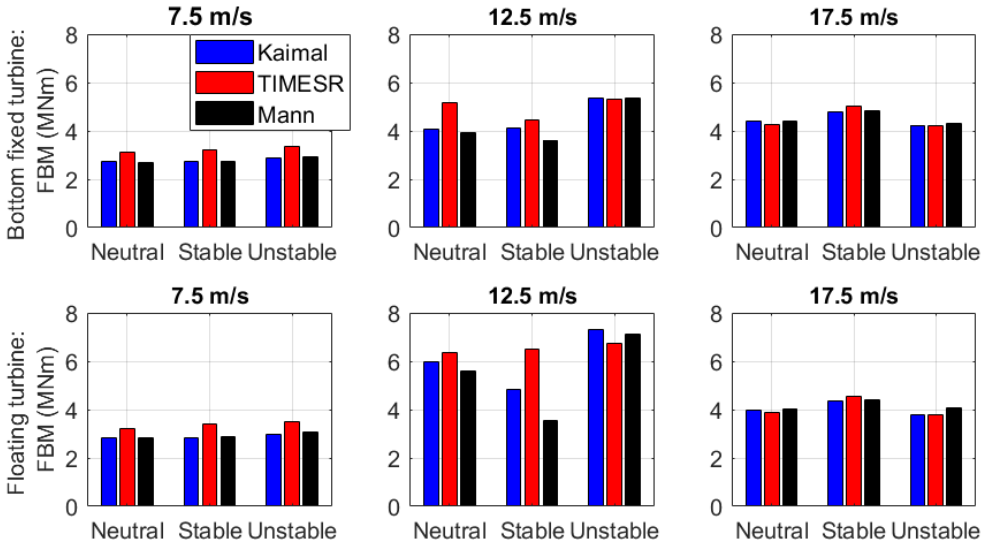

Figure 11. Standard deviation of flap-wise bending moment (FBM) in MNm. Results by considering various atmospheric stabilities and wind field simulation methods. 7.5 m/s, 12.5 m/s and 17.5 m/s mean wind speeds. Bottom fixed turbine (top) and floating turbine (bottom).

In Figure 12 examples of the load spectra for the FBM are presented for the bottom fixed and floating turbine respectively. As for the TTBM, the FBM exhibits very distinct peaks in the load spectra for the bottom fixed turbine as seen in Figure 12. The most distinct peak is at 1P (0.16 Hz), as can be expected following the rotation of a single blade. However, also clear peaks are observed at 2P and 3P and at frequencies close to the 1st blade flap mode (0.59 Hz) and the collective blade flap mode (0.64 Hz).

As for the TTBM, the distinct peaks in the response are smoothed out in the case of the floating turbine. Again, it is assumed that the motion of the floater causes a damping effect to the resonant motions. From Figure 11 (centre) it is observed that the Mann formulation of the wind spectrum gives the lowest FBM, in particular in stable atmospheric conditions. From Figure 12, it is observed that the differences are mainly due to the response at low frequencies. As the TI level and wind shear are similar for the three wind field generation methods applied, it seems likely that the difference is due to the differences in the coherence of the wind fields, see Figure 6.

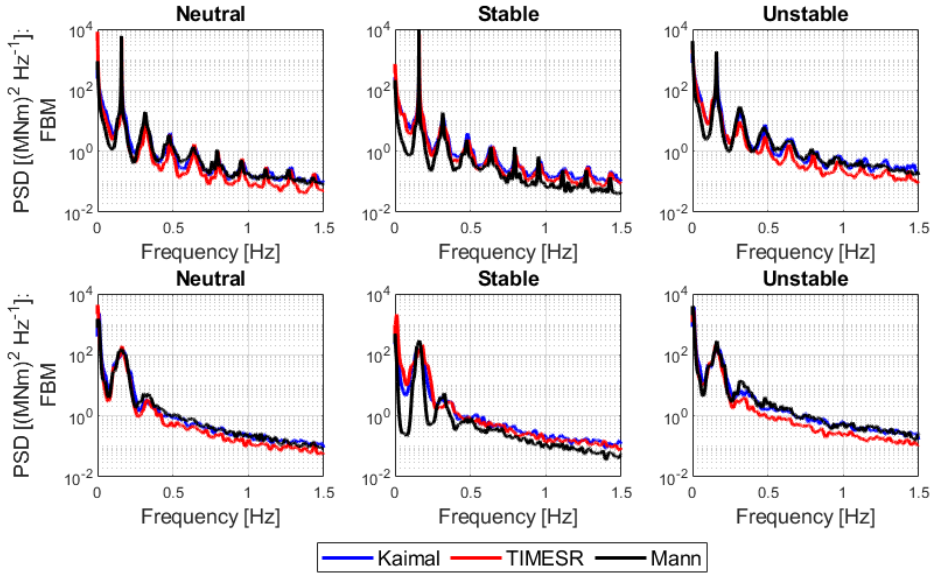

Figure 12. Load spectra for the blade flap-wise bending moment (FBM) for 12.5 m/s mean wind speed. Bottom fixed turbine (top) and floating turbine (bottom). Neutral (left), stable (centre) and unstable (right) atmospheric conditions.

3.2.4. Tower top yaw moment. The yaw motion of the floater, discussed in Chapter 2.3, does not have any impact in the TTYM. Thus, we see from Figure 13 that the results of the TTYM are similar for the bottom fixed and floating wind turbine. The standard deviations for the TTYM in Figure 13 show a similar behaviour as for the previous results: the largest variations between atmospheric stability classes and wind field generation methods are found at the 12.5 m/s wind speed.

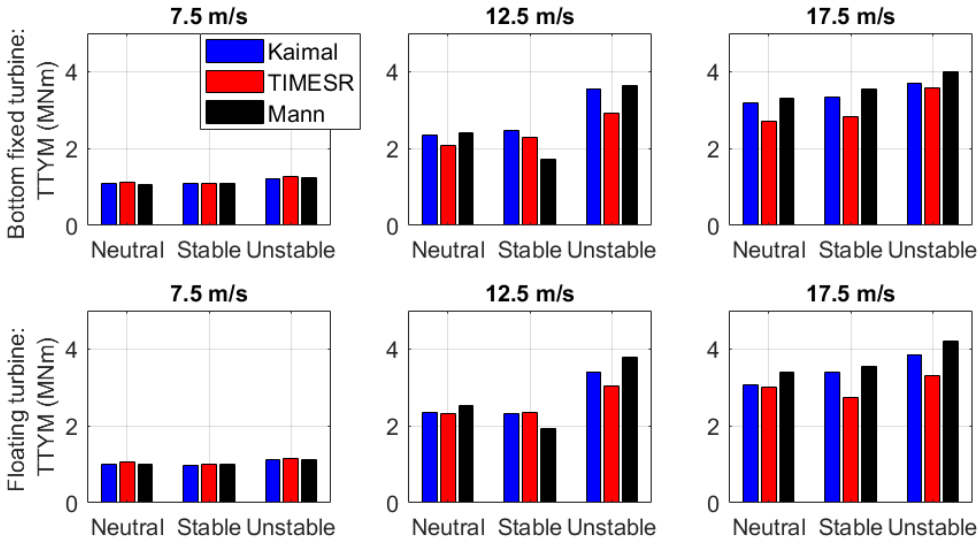

Figure 13. Standard deviation of tower top yaw moment (TTYM) in MNm. Results by considering various atmospheric stabilities and wind field simulation methods. 7.5 m/s (left), 12.5 m/s (centre) and 17.5 m/s (right) mean wind speeds. Bottom fixed turbine (top) and floating turbine (bottom).

The Mann formulation gives in general higher loads than Kaimal and TIMESR in the TTYM compared to the other responses discussed above. A possible explanation is the low coherence in lateral direction of the Mann wind field, Figure 6, causing larger yaw moments. Also, the no-zero quad-coherence, Figure 5, will contribute to the yaw moment.

The load spectra in Figure 14 show similar frequency content as the TTBM. For the bottom fixed turbine, the narrow peak at 0.16 Hz correspond to 1P with the exception in the unstable condition where it is not as clear. Further, we see the 3P frequency (0.48 Hz) and the various blade modes (0.96 Hz and 1.43 Hz), see Table 4.

The load spectra for the floater clearly demonstrate the rotational peaks, 1P and 3P at 0.16 Hz and 0.48 Hz. The blade mode peak at 0.96 Hz are not as distinct as we observed for the bottom fixed turbine.

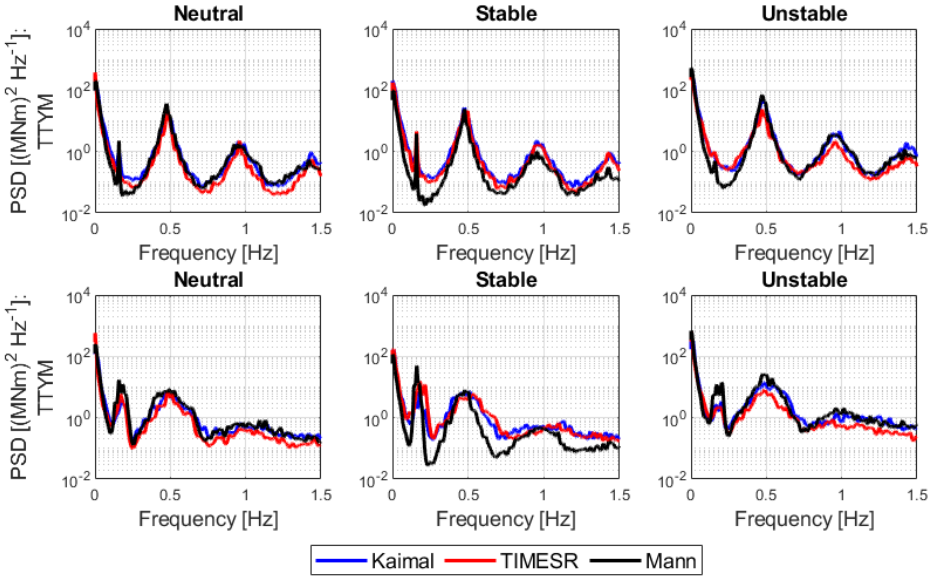

Figure 14. Load spectra for the tower top yaw moment (TTYM) for 12.5 m/s mean wind speed. Bottom fixed turbine (top) and floating turbine (bottom). Neutral (left), stable (centre) and unstable (right) atmospheric conditions.

4. Conclusions

In the present work, various methods for generating an incident wind field to large diameter offshore wind turbines has been discussed. Three different methods have been used, the Mann uniform shear model, the Kaimal wind spectrum formulation as well as a method using measured wind time histories as input together with an exponential coherence model (TIMESR). The loads on a bottom fixed and a floating wind turbine are studied at wind velocities below rated, close to rated and above rated wind speeds. Three different atmospheric stabilities are considered in each case.

Analyses of the coherence of the wind fields, show that the various methods exhibit very different behaviour. The Mann model as well as analyses of point measurements, shows that the co-coherence may have negative values and the quad-coherence may be non-zero. This contrasts what is assumed using the commonly accepted exponential co-coherence model used together with the Kaimal model. The difference in coherence has consequences for global loads on the wind turbines. It is e.g. probable that the Mann model at above rated wind speed gives higher standard deviations in yaw than the two other methods, based upon exponential coherence models, due to the lower co-coherence and phase

shifts present. This is observed both for the bottom fixed and floating turbine. The various response parameters considered are to a different degree sensitive to the wind spectra and coherence model.

At below and above rated wind speeds the various stability classes do not show very large differences in tower bottom bending moments. However, close to rated wind speed, the unstable atmospheric condition seems to cause larger dynamic tower bottom bending moments than the neutral and stable conditions. The various wind field models give also large variation in the dynamic loads. In general, the tower bottom bending moment for the floater is larger than for the bottom fixed turbine.

The results for the tower top bending moments, the blade root flapping moment as well as the tower top yaw moment exhibit somewhat similar behaviour as the tower bottom bending moment. However, the significant differences between the fixed and floating turbine in the tower bottom bending moment is not seen for the other results. In the floater case, the rigid body motions and controller settings seem to smooth out several of the sharp, resonant peaks in the power spectra of the loads observed for the bottom fixed turbine. This study concludes that the atmospheric turbulence, stability and coherence all are important to the dynamic response of a wind turbine.

Acknowledgement
Etienne Cheynet, UiB, is acknowledged for his many advises and suggestions in processing and interpreting data. Marte Godvik, Equinor, is acknowledged for her advises and Phani Manne for his support during the work with the master thesis of Maylinn Myrtvedt, being the basis for the present article.

References

[1] FINO-1, 'FINO1 - research platform in the North Sea and the Baltic No. 1'. [Online]. Available: https://www.fino1.de/en/. [Accessed: 13-Apr-2019].
[2] A. Nybø, F. G. Nielsen, and J. Reuder, 'Processing of sonic anemometer measurements for offshore wind turbine applications', *J. Phys. Conf. Ser.*, vol. 1356, p. 13, 2019.
[3] L. Eliassen and C. Obhrai, 'Coherence of Turbulent Wind under Neutral Wind Conditions at FINO1', in *Energy Procedia*, 2016.
[4] A. Nybø, F. G. Nielsen, J. Reuder, M. J. Churchfield, and M. Godvik, 'Evaluation of different wind fields for the investigation of the dynamic response of offshore wind turbines', *Wind Energy*, pp. 1–21, 2020.
[5] C. Bak *et al.*, 'The DTU 10-MW Reference Wind Turbine', p. 22, 2013.
[6] M. Godvik, 'Influence of wind coherence on the response of a floating wind turbine'. .
[7] I. E. Commision, 'IEC 61400-1:2019 Wind energy generation systems - Part1: Design requirements.', 2019. [Online]. Available: https://webstore.iec.ch/publication/26423. [Accessed: 02-Jan-2020].
[8] I. E. Commision, 'IEC TS 61400-3-2:2019. Wind energy generation systems - Part 3-2: Design requirements for floating offshore wind turbines.', 2019. [Online]. Available: https://webstore.iec.ch/publication/29244. [Accessed: 02-Jan-2020].
[9] I. E. Commision, 'IEC 61400-3-1:2019 Wind energy generation systems - Part 3-1 Design requirements for fixed offshore wind turbines', 2019. [Online]. Available: https://webstore.iec.ch/publication/29360. [Accessed: 02-Jan-2020].
[10] A. G. Davenport, 'The spectrum of horizontal gustiness near the ground in high winds', *Q. J. R. Meteorol. Soc.*, vol. 87, no. 372, pp. 194–211, 1961.
[11] M. H. Myrtvedt, 'Investigation of the importance of wind field modelling for loads on a bottom fixed and a spar floater wind turbine', University of Bergen, 2019.
[12] A. J. M. Van Wijk, A. C. M. Beljaars, A. A. M. Holtslag, and W. C. Turkenburg, 'Evaluation of stability corrections in wind speed profiles over the North Sea', *J. Wind Eng. Ind. Aerodyn.*, vol. 33, no. 3, pp. 551–566, 1990.
[13] A. Sathe, J. Mann, T. Barlas, W. A. A. M. Bierbooms, and G. J. W. Van Bussel, 'Influence of atmospheric stability on wind turbine loads', *Wind Energy*, vol. 16, no. 7, pp. 1013–1032, 2012.
[14] B. J. Jonkman, 'TurbSim User's Guide v2. 00.00', *Natl. Renew. Energy Lab.*, 2014.
[15] 'DTU Wind Energy Pre-processing tools'. [Online]. Available: http://www.hawc2.dk/download/pre-processing-tools. [Accessed: 05-Jul-2019].

[16] R. B. Stull, *An introduction to Boundary Layer Meteorology*. Kluwer academic publishers, 1988.
[17] DNV GL, 'Sesam: Software suite for hydrodynamic and structural analysis of ships and offshore structures', 2019.
[18] S. H. Sørum, J. T. H. Horn, and J. Amdahl, 'Comparison of numerical response predictions for a bottom-fixed offshore wind turbine', *Energy Procedia*, vol. 137, p. 11, 2017.
[19] S. H. Sørum, J. R. Krokstad, and J. Amdahl, 'Wind-wave directional effects on fatigue of bottom-fixed offshore wind turbine', *J. Phys. Conf. Ser.*, vol. 1356, p. 13, 2019.
[20] W. Xue, 'Design, numerical modelling and analysis of a spar floater supporting the DTU 10MW wind turbine', p. 114, 2016.
[21] Morten Hartvig Hansen ; Lars Christian Henriksen, *Basic DTU Wind Energy controller*. 2013.
[22] H. A. Panofsky and I. A. Singer, 'Vertical structure of turbulence', *Q. J. R. Meteorol. Soc.*, vol. 91, no. 389, pp. 339–344, 1965.
[23] E. E. Bachynski and L. Eliassen, 'The effects of coherent structures on the global response of floating offshore wind turbines', *Wind Energy*, vol. 22, no. 2, pp. 219–238, 2019.
[24] N. Dimitrov, A. Natarajan, and J. Mann, 'Effects of normal and extreme turbulence spectral parameters on wind turbine loads', *Renew. Energy*, vol. 101, pp. 1180–1193, 2017.
[25] P. Doubrawa, M. J. Churchfield, M. Godvik, and S. Sirnivas, 'Load response of a floating wind turbine to turbulent atmospheric flow', *Appl. Energy*, vol. 242, pp. 1588–1599, 2019.